Magnetostructural features of phase transitions in the $Mn_{1-x}Co_xNiGe$ system Part 2. Analysis

© V.I. Mitsiuk[1], G.S. Rimskiy[1], V.V. Koledov[2], A.V. Mashirov[2], V.I. Val'kov[3], A.V. Golovchan[3], O.E. Kovalev[3]

[1] Scientific and Practical Materials Research Center, National Academy of Sciences of Belarus,
Minsk, Belarus
[2] Kotelnikov Institute of Radio Engineering and Electronics, Russian Academy of Sciences,
Moscow, Russia
[3] Galkin Donetsk Institute for Physics and Engineering,
Donetsk, DPR, Russia

E-mail: valkov09@gmail.com

Within the framework of the model of interacting parameters of the magnetic and structural orders, taking into account the internal periodic magnetic field orthogonal to the exchange field, we analyzed the features of magnetostructural transitions in the $Mn_{1-x}Co_xNiGe$ system. A qualitative description of changes in the nature of magnetic phase transitions from magnetostructural transitions of the 1st order paramagnetism-antiferromagnetism ($x = 0.05-0.1$) to isostructural transitions of the 2nd order paramagnetism-ferromagnetism ($x = 0.15-0.8$) with a change in the concentration of Co is presented. An explanation is given for the onset of irreversible magnetic-field-induced transitions at temperatures on the order of 5 K in strong magnetic fields, accompanied by a change in the saturation magnetization for samples $x = 0.15-0.8$. The low-temperature inverse magnetocaloric effect at liquid helium temperatures is predicted for these samples.

Keywords: irreversible magnetostructural first-order phase transition, helimagnetism, direct and inverse magnetocaloric effects.

DOI: 10.21883/PSS.2022.14.54334.153-2

1. Introduction

As established in the first part of our work, magnetic disordering in the $Mn_{1-x}Co_xNiGe$ system, depending on the Co concentration, is realized as the 1st or 2nd order magnetic phase transitions. In samples with $x = 0.05$ and $x = 0.1$ with a high-temperature paramagnetic (PM) phase with a hexagonal (hex) crystal structure of the Ni_2In type (space group $P6_3/mmc$), a decrease of the temperature leads to a magnetostructural 1st order transition and stabilization of the antiferromagnetic (AF) phase with an rhombic crystal structure of the TiNiSi type (space group P_{nma}). With an increase in the concentration of Co in samples with $x = 0.15-0.80$, the observed high-temperature magnetic phase transitions are isostructural transitions of the 2nd order $PM(P6_3/mmc) \leftrightarrow FM(P6_3/mmc)$. In this case, the saturation magnetization of the hexagonal ferromagnetic phase FM(hex) decreases with increasing concentration x. Other peculiarities of samples with $x = 0.15-0.80$ include anomalous sensitivity of magnetization to measurements in the ZFC, FC modes in magnetic fields with induction up to 5 T.

To analyze the mechanisms of the nontrivial behavior of the samples of the system under study, the model of interacting parameters of the magnetic and structural orders [1,2], supplemented by taking into account the internal orthogonal field that regulates the change in the ratio between the values of the saturation magnetization of the rhombic and hexagonal phases, was applied.

2. Analysis of magnetic phase transitions in the $Mn_{1-x}Co_xNiGe$ system based on the model of interacting parameters of the structural and magnetic orders

Thermodynamic potential (TP) $\Omega \equiv \Omega(Q_0, \sigma, e_1, e_2, y)$ of a magnetoelastic system in which a structural transition of the „displacement" type $hex(P6_3/mmc) \rightarrow orth(P_{nma})$, can be formally represented as the TP sum of the structural $\Omega_1 \equiv \Omega_1(Q_0, \sigma, e_1, e_2)$ and the spin $\Omega_2 \equiv \Omega_2(\hat{H}(\hat{s})) = \Omega_s(y)$ subsystems.

$$\Omega = \Omega_1 + \Omega_2. \tag{1}$$

For the theoretical analysis of such magnetostructural systems, we use a model in which the spontaneous appearance of rhombic symmetry and the corresponding configuration of atoms in the crystal lattice is associated with the freezing of optical vibrations of Ni atoms below the temperature T_{t1} [1,2]. According to [1,3], the thermodynamic potential

(TP) of a structurally elastic subsystem has the form

$$
\Omega_1(Q_0, \sigma, e_1, e_2) = \frac{N_0}{2} V_0(Q_0^2 + \sigma) + \frac{N_0}{4}(\gamma Q_0^4 + 6Q_0^2\sigma + 3\sigma^2)
$$
$$
+ \frac{N_0}{6}\Gamma(Q_0^6 + 15Q_0^4\sigma + 45Q_0^2\sigma^2 + 15\sigma^3)
$$
$$
- \frac{1}{2}N_0 Q_0^2 v_0(1 + L_1 e_1 + L_2 e_2) - T\frac{k_B}{2}N_0\ln\sigma
$$
$$
+ \frac{1}{2}e_1^2 k_0 + \frac{1}{2}(e_2)^2 k_2 + Pe_1 - T\alpha e_1 k_0. \tag{2}
$$

Average value in the approximation of a shifted harmonic oscillator [3]

$$
Q_0 = \langle Q_n \rangle = \int_{-\infty}^{\infty} \frac{1}{\sqrt{2\pi\sigma}} \exp\left[\frac{-(Q_n - Q_0)^2}{2\sigma}\right] Q_n \, dQ_n,
$$

describing the frozen shared shift Q_n of Ni_1, $Ni_2 \langle U_{nz}^{Ni1,2}\rangle$ ions in the n-th lattice cell during the structural transition $P6_3/mmc\,(Q_0 = 0) \leftrightarrow P_{nma}\,(Q_0 \neq 0)$, is identified with the structural order parameter. The average value Q_0 and the dispersion $\sigma = \langle[Q_n - Q_0]^2\rangle$ are considered as independent variational parameters and are determined from the minimization of the total thermodynamic potential of the magnetoelastic system Ω. Dependence of the Fourier component of pair-wise interaction between soft modes of different cells

$$
v_0(e_1, e_2, x) = \sum_{n'} v_{nn'} = v_0(x)(1 + L_1 e_1 + L_2 e_2)
$$

from volume (e_1) and rhombic (e_2) strains and concentration (x) takes into account the connection of the phonon subsystem with the static strains of the crystal and the chemical composition $(L_1 = (\partial v_0/\partial e_1)/v_0(x), \quad L_2 = (\partial v_0/\partial e_2)/v_0(x))$. Since with increasing Co concentration, the volume V_{hex} of the hexagonal cell decreases, and the appearance of the structural order parameter at the transition hex$[P6_3/mmc\,(Q_0 = 0)] \leftrightarrow$ orth$[P_{nma}\,(Q_0 \neq 0)]$ is followed by its increment $((V_{orth} - V_{hex})/V_{hex} \equiv \Delta V/V = e_1 > 0)$, then $L_x = (\partial v_0/\partial e_1)(\partial e_1/\partial x)/v_0 < 0$. Thus, an increase in x can be compared with an increase in internal „chemical" pressure.

The spin subsystem includes magnetically active Mn atoms with spin magnetic moment $2\mu_B \hat{s}_n^k$ (μ_B — Bohr magneton). At the $P6_3/mmc\,(Q_0 = 0) \leftrightarrow P_{nma}\,(Q_0 \neq 0)$ structural transition, these atoms are also displaced from their previous equilibrium positions, however, these shifts, which arise due to shifts of Ni atoms, cannot be attributed to local (relating to a specific cell n). Thus, as a result of a structural transition, it can be spoken about a change in the complete configuration of the atomic system, which, through a change in the spin-polarized electron structure, leads to a change in the main magnetic characteristics of the system. And not only the type of magnetic ordering,

but also the magnitude of the saturation magnetization and the magnitude of the effective magnetic moment [4]. This is naturally taken into account in first-principles approaches [4]. However, within the phenomenological approaches based on the Heisenberg model, which initially uses localized magnetic moments, the spin state change factor requires special approaches. For example, a change in the measured value of the saturation magnetic moment while maintaining the value of the atomic spin can be described in terms of a model of the Heisenberg type with the introduction of an internal field orthogonal to the direction of the measured magnetic moment. For spin systems with a spatially periodic structure, this internal field $\mathbf{O}_n^k$ is also spatially periodic. In this case, to describe a simple spatially periodic helimagnetic spin structure with a wave vector of the structure $\mathbf{q} = [0, 0, q_a]$ [5], the Hamiltonian of the spin subsystem can be represented as

$$
\hat{H}(s) = -\sum_{nk,n'k'} J_{nn'}^{kk'} \hat{s}_n^k \hat{s}_{n'}^{k'} - 2\mu_B \mathbf{H}_0 \sum_{ni} \hat{s}_n^k - \sum_{ni} \mathbf{O}_n^k \hat{s}_n^k. \tag{3}
$$

where $\hat{s}_n^k$ — are spin operators of k-atoms in the n-th elementary hexagonal cell, $J_{nn'}^{kk'} \equiv J(|\Delta \mathbf{R}_{nn'}^{kk'}|)$ corresponding integrals of the exchange interaction between magnetically active atoms at a distance

$$
|\Delta \mathbf{R}_{nn'}^{kk'}| = |\mathbf{R}_n^{k'} - \mathbf{R}_n^k| \equiv D(Q_0, e_1), \tag{4a}
$$

$\sum_n = N_0$, $\sum_{n,k} = N = 2N_0(1 - x)$ — number of elementary cells and number of magnetically active atoms (Mn) per unit volume, and $\mathbf{O}_n^k = \mathbf{w}_n^k O$, $\mathbf{H}_0 = [0, 0, H_0]$ — vectors of internal spatially periodic and external homogeneous magnetic fields, μ_B — Bohr magneton; $\mathbf{w}_n^k$ — the unit vector that determines the direction of the space-periodic field $\mathbf{O}_n^k$ with modulus O is given by

$$
\mathbf{w}_n^k = [\sin(\mathbf{q}\mathbf{R}_n^k), -\cos(\mathbf{q}\mathbf{R}_n^k), 0]. \tag{4b}
$$

In the mean field approximation (MFA), the thermodynamic potential of the spin system $\Omega_2(\hat{\mathbf{H}}(\hat{s}))$ with the Hamiltonian (3) can be reduced to $\Omega_s(y) \equiv \Omega_M$ (Appendix)

$$
\Omega_2(\hat{\mathbf{H}}(\hat{s})) = \Omega_s(y)
$$
$$
= N[J(q_a)\sin(\vartheta)^2 + J(0)\cos(\vartheta)^2]y^2 s^2 - Nk_B T \ln z(X), \tag{5a}
$$
$$
J(q_a) \approx J_0(Q_0, e_1) + J_1(Q_0, e_1)\cos(\Psi)
$$
$$
+ J_2(Q_0, e_1)\cos(2\Psi), \tag{5b}
$$
$$
J(0) \approx J_0(Q_0, e_1) + J_1(Q_0, e_1) + J_2(Q_0, e_1). \tag{5c}
$$

$\Psi = q_a c_{hex}/2$, $2\Psi = q_a c_{hex}$ — parameters of the helicoidal structure described by the wave vector q_a; $J_0(Q_0, e_1)$ — interatomic exchange integrals between Mn atoms inside layers perpendicular to the direction of the wave vector $\mathbf{q}$; $J_1(Q_0, e_1)$ and $J_2(Q_0, e_1)$ interatomic exchange integrals between Mn atoms located in the nearest and next to the nearest layers at distances $c_{hex}/2$ and c_{hex} (c_{hex} — hexagonal

cell parameter along wave vector direction $\mathbf{q}$); ϑ — angle between the direction of the local quantization axis and the direction of the external field $\mathbf{H}_0$; k_B — Boltzmann constant.

The dependence of the exchange interaction integrals $J(q_a)$ on the structural order parameter Q_0 and volume strain e_1, which follows from condition (4a), ensures the interaction between the spin and structural subsystems via the relation between the parameters of the magnetic y and structural orders

$$y = m/s \leq 1, \qquad (6)$$

$m = \langle \hat{s}_n^k \mathbf{u}_n^k \rangle_h \equiv \langle \hat{m}_n^k \rangle_h$ is the mean value of the spin projection $\hat{m}_n^k$ to the direction of the local quantization axis

$$\mathbf{u}_n^k = \left[\cos(\mathbf{q}\mathbf{R}_n^k)\sin(\vartheta), \ \sin(\mathbf{q}\mathbf{R}_n^k)\sin(\vartheta), \ \cos(\vartheta) \right],$$

calculated in the mean field approximation (Appendix)

$$z(X) = \text{sh}\left[\left(1 + (2s)^{-1}\right)X\right] / \text{sh}\left[(2s)^{-1}X\right], \qquad (7)$$

$$X = \frac{1}{k_B T} \sqrt{ \begin{array}{l} \{[J(q_a)\sin^2(\vartheta) + J(0)\cos^2(\vartheta)]ys^2 + \\ + 2\mu_B H_0 s \cos(\vartheta)\}^2 + O^2 s^2 \end{array} }, \qquad (8)$$

The extremum of the function $J(q_a)$ is determined from the equation $\partial J(\Psi)/\partial \Psi = 0$, the competing solutions of which for $J_1(Q_0, e_1) > 0$, $J_2(Q_0, e_1) < 0$ will only be helicoidal (for $\cos \Psi = J_1(Q_0, e_1)/4|J_2(Q_0, e_1)| = \delta(Q_0) \equiv \delta < 1$) with a higher value quantities $J(q)$ ($J(q) = J_0(Q_0, e_1) + (2\delta^2 + 1)|J_2(Q_0, e_1)|$) and ferromagnetic (at $\Psi = 0$) with lower magnitude $J(0)$ ($J(0) = J_0(Q_0, e_1) + (4\delta - 1)|J_2(Q_0, e_1)|$) since $\Delta J \equiv J(q) - J(0) = 2(\delta - 1)^2 |J_2(Q_0, e_1)| > 0$.

For subsequent calculations, the values $J(q_a)$, $J(0)$ can be represented as an expansion in linear powers of volumetric strains e_1 and even powers of structural order parameters Q_0^{2n}, as well as their combinations in the form $(e_1 Q_0^2)^n$. In this work, we will only take into account the expansion terms up to Q_0^4 and linear combinations $(e_1 Q_0^2)$. Such a decomposition does not contradict physical considerations and keeps the TP invariant in association with operations of the symmetry group $P6_3/mmc$. Then the value $J(q_a)\sin^2(\vartheta) + J(0)\cos^2(\vartheta) \equiv J(q_a) - \Delta J \cos^2(\vartheta)$ in (5) and (8) can be represented as

$$J(q_a) - \Delta J \cos^2(\vartheta) = J_{00}\big[r_{AF} + Q_0^2(\lambda_{AF} + \lambda_{1AF}e_1)2$$
$$+ 2\lambda Q_0^4 - \Delta J \cos^2(\vartheta)\big], \qquad (9)$$

$$\Delta J \equiv J(q_a) - J(0) = J_{00}\big[1 + 2Q_0^2(\lambda_{20} + \lambda_{21}e_1)\big]$$
$$\times \big[2z(\cos\Psi - 1)(2\delta(Q_0) - \cos\Psi - 1)\big], \qquad (10a)$$

$$r_{AF} = 1 + z\big[4\delta(Q_0)\cos\Psi - 2\cos^2\Psi + 1\big], \qquad (10b)$$

$$\delta(Q_0) = R - AQ_0^2 + BQ_0^4, \qquad (10c)$$

$$\lambda_{AF} = \lambda_{00} + z\lambda_{20}\big[4\delta(Q_0)\cos\Psi - 2\cos^2\Psi + 1\big]. \qquad (10d)$$

$$\lambda_{1AF} = \lambda_{01} + z\lambda_{21}\big[4\delta(Q_0)\cos\Psi - 2\cos^2\Psi + 1\big], \qquad (10e)$$

$$J_{00} \equiv J_0(Q_0 = e_1 = 0) = 3T_0 k_B / 2s(s + 1). \qquad (10f)$$

The temperature dependences of the magnetic, structural, and elastic characteristics can be obtained from the conditions for the extreme value of the thermodynamic potential: $\partial J(q_a)/\partial \Psi = 0$, $\partial\Omega/\partial\vartheta = 0$, $\partial\Omega/\partial\sigma = 0$, $\partial\Omega/\partial e_1 = 0$, $\partial\Omega/\partial e_2 = 0$, $\partial\Omega/\partial y = 0$, $\partial\Omega/\partial Q_0 = 0$. The first two equations determine the conditions for the existence of a helimagnetic structure regardless of the external magnetic field (11a) and in the external magnetic field $\mathbf{H}_0 = [0, 0, H_0]$, (11b)

$$\cos\Psi = \begin{cases} \delta(Q_0) & \text{at } |\delta(Q_0)| < 1 \\ 1 & \text{otherwise} \end{cases}, \qquad (11a)$$

$$\cos\vartheta = \begin{cases} \dfrac{2H_0\mu_B}{(J(q_a) - J(0))y} & \text{at } |\delta(Q_0)| < 1 \\ \dfrac{2H_0\mu_B}{(J(q_a) - J(0))y} & \text{at } \left|\dfrac{2H_0\mu_B}{(J(q_a) - J(0))y}\right| < 1 \\ 1 & \text{otherwise.} \end{cases}$$
$$(11b)$$

The following three equations have analytical solutions in the form of dependencies: $e_1 = e_1(Q_0, y, T, P)$, $e_2 = e_2(Q_0)$, $\sigma = \sigma(Q_0, T)$. The last two of them are reduced to the form

$$-y^2(\partial h_m/\partial Q_0) + (\partial\Omega_1(Q_0, \sigma, e_1, e_2)/\partial Q_0) = 0, \quad (12a)$$

$$y - B_s(X)\frac{(2a/a_3)h_m y + 2\mu_B s H_0 \cos\vartheta}{\sqrt{((2a/a_3)h_m y + 2\mu_B s H_0 \cos\vartheta)^2 + s^2 O^2}} = 0, \qquad (12b)$$

$$X = \left[\sqrt{[(2a/a_3)h_m y + 2\mu_B s H_0 \cos\vartheta]^2 + s^2 O^2}\right] / k_B T, \qquad (12c)$$

$$ah_m \equiv ah_m(Q_0, e_1) \equiv ah_m(Q_0, y, T, P)$$
$$= NJ_{00}\big(J(q)/J_{00} - \Delta J(q)\cos\vartheta^2/J_{00}\big)s^2. \qquad (12d)$$

$$a = NJ_{00}s^2 = (3/2)s^2 a_3 T_0/s(s + 1),$$
$$a_2 = N_0 k_B = 2(1 - x)a_3, \quad a_3 = Nk_B.$$

$B_s(X)$ — Brillouin function:

$$B_s(X) = \left(\frac{1}{2s + 1}\right)\coth\left(\frac{X}{2s + 1}\right) - \left(\frac{1}{2s}\right)\coth\left(\frac{X}{2s}\right)$$
$$= B_s(Q_0, y, T, P) \qquad (13)$$

In (12) we use the following expression

$$v_0(x)(1 + L_1 e_1 + L_2 e_2) \equiv v_0(1 + L_x x)(1 + L_1 e_1 + L_2 e_2)$$
$$\text{at } L_x < 0. \qquad (14)$$

Equations (12) are solved numerically and allow to obtain the temperature dependences of the magnetic ($y(T)$) and structural ($Q_0(T)$) order parameters in the presence of pressure P and an external magnetic field H_0 depending

on the concentration x and the modulus of the internal periodic field $O(x) = |\mathbf{O}_n^k|$. Condition (11b), taking into account expression (10c) for $A > 0$, $B > 0$, in accordance with calculations [4] and experimental data [5,6], identifies the appearance of a helimagnetic structures only in the rhombic state.

The dependences $y(T)$ and $Q_0(T)$ determine the behavior of the temperature dependences of the magnetization $M(T)$ for given values of the magnetic field strength H_0 and the dimensionless inverse paramagnetic susceptibility $\chi^{-1}(T)$ within $H_0 \to 0$

$$M(T) = M_0(x)y(T)\cos\vartheta(T), \qquad (15a)$$

$$\chi^{-1}(T, P) = \frac{a_3 O(x) - 2aB_s(Q_0, 0, T, P)h_m(Q_0, 0, T, P)}{2aB_s(Q_0, 0, T, P)}, \qquad (15b)$$

where $M_0(x)$ — saturation magnetization in the model of localized Mn spins for a sample with a given number x and spin $s = 3/2$; to calculate it, we use the expression

$$M_0[\text{emu/g}] = (1-x)2s\mu_B/A(x)$$
$$= 1.116906^* s^* 10000^* (1-x)/A, \qquad (16)$$

A — atomic weight per formula unit.

For example, for samples with x: 0.05; 0.1; 0.15; 0.8; 0.7 $M_0(x)$ values reach 85.37; 80.79; 76.22; 71.22; 62.56 emu/g respectively. In the usual model of a ferromagnet with localized spins, these values correspond to the saturation magnetization, since at $T = 0$, $y = \cos\vartheta = 1$. However, in the case under consideration, for $O(x) \neq 0$ and the parameter $O(x)$ increases with growth x, the values of $M(T = 0)$ to the maximum achievable magnetic fields, in full agreement with the experimental results [7] are far from the values of $M_0(x)$. Meanwhile, as will be shown below, the solution of the equations of state (12), depending on the ratio between the values of the quantities $O(x)$, $v_0(x)$, and $(2a/a_3)h_m$, leads to two radically different scenarios of the behavior of magnetostructural characteristics. These scenarios can be compared with the results given in Part 1 of this work [7] in Fig. 6, a, b and Fig. 6, c, d.

The table gives the values of the thermodynamic potential coefficients, which are used to solve the equations of state (12) and then compare the results of the solutions and the experimental results of measurements of samples with the corresponding concentrations x. The values a_2, a_3 are calculated based on the X-ray density $\rho(x)$, table [7]. The quantities $M_0(x)$ are calculated for the spin $s = 3/2$ by the formula (16).

First, based on the solutions of equations (12) with the corresponding values of the coefficients, we will give an interpretation of the experimental peculiarities of the magnetic measurements of $Mn_{1-x}Co_xNiGe$ solid solutions for samples with $x < 0.15$.

Meanwhile, we will proceed from the following: in the area of anomalous behavior of the inverse paramagnetic susceptibility (see Fig. 5,6 in [7]), there is magnetostructural transition of the 1st order PM(hex) $\leftrightarrow$ HM(orth) at temperatures $T_t \approx 250-300$ K significantly higher than the paramagnetic instability temperature of the hexagonal phase $T_t > \theta_{\text{hex}} \approx 100-150$ K.

According to the theoretical analysis, this becomes achievable with an appropriate selection of the TP coefficients (table). Then, Fig. 1, a, b, c, the calculated value of the lability temperature of the hexagonal phase exceeds the paramagnetic Curie temperature of the orthorhombic phase: $T_{t1} \geq \theta_{\text{orth}}$. The instability temperature of the hexagonal phase in this case can coincide with the temperature of the initiation of helimagnetic order $T_{t1} = T_{N1}$. As a result of the interrelation of these processes, the magnetic ordering becomes a magnetostructural transition of the 1st order PM(hex) $\leftrightarrow$ HM(orth), which is accompanied by an abrupt change in the magnetization M_{orth}, temperature hysteresis $\Delta T = T_{t2} - T_{t1}$, anomalous behavior of the reverse magnetic susceptibility $\chi^{-1}(T)$, which is consistent with the experimental dependences, Fig. 1, d, e, f. This behavior corresponds to the first scenario.

The difference between the shapes of the experimental $\sigma(T)$ and theoretical $M_{\text{orth}}(T)$ dependences is not significant and is related to the orientation factor: in the experiment with polycrystalline powder, the direction of the magnetic field vector $\mathbf{H}$ and the direction of the wave vector of the magnetic structure $\mathbf{q}$ is not fixed; in theory, a strict condition for the collinearity of both vectors is under study. It should be noted that the temperature dependences of the magnetization $M_{\text{orth}}(T)$ and the magnetic order parameter $y(T)$ ($M_0y(T)$ in Fig. 1, a) also differ qualitatively. The dependence $y(T)$ reflects the change in the magnitude of the magnetic moment in the rhombic phase along the local space-periodic quantization axis and can only be studied in experiments on magnetic neutron scattering; the temperature dependences of the magnetization in the $M_{\text{orth}}(T)$ orthorhombic phase are fixed as a response of a helimagnetic space-periodic structure to an external spatially uniform magnetic field, i.e., as a distortion of the helimagnetic structure. The paramagnetic Curie temperature θ_{hex} for the hexagonal phase is determined from the extrapolation of the high-temperature dependence of the inverse paramagnetic susceptibility $\chi_{\text{hex}}^{-1}(T)$ measured in the hexagonal phase. The PM Curie temperature of the θ_{orth} orthorhombic phase in the case of the 1st order transition under consideration is an unobservable value, since the appearance of the helimagnetic order occurs abruptly at $T_{t1} = T_{N1} < \theta_{\text{orth}}$. However, in a real experiment, in which magnetostructural transitions are close to diffuse first-order phase transitions, the value of θ_{orth} can be compared with the temperature θ^* in Fig. 1, f.

In strong magnetic fields, the distortion of the helimagnetic structure is so significant that it can be spoken of its complete suppression over the entire temperature range, Fig. 2, d, e, f. From the curves shown in Fig. 2, a, b, c it can be seen that as the magnetic field increases, the temperature dependences of $\cos\vartheta$ approach their saturation-1, which

Change in the main TP coefficients in describing the magnetostructural properties of alloys of the $Mn_{1-x}Co_xNiGe$ system

x	$\nu_0(x)$	sO/k_B at $s=3/2$	λ_{00}	λ_{20}	$L3$	$\dfrac{\lambda_{AF}^{max}}{\lambda_{AF}^{min}}$	T_0	A	B	M_0	a_2	a_3
unit	kbar	K					K			emu/g	kbar	
0.05	47.56	282.5	1	34.5	7.0	99.7 / 95.7	40	6.2	57	85.12	0.00177	0.00337
0.1	43.62	382.5	1	22	7.0	68.09 / 67.58	50	6.2	70	80.56	0.00178	0.00321
0.15	37.47	467.5	7.0	−1.76	19	1.82 / 1.52	69.0	6.2	20	76	0.0018	0.00306
0.2	37.47	520	7.7	−1.76	18	1.8	74	6.2	20	71.6	0.0018	0.00289

N o t e. The values a_2, a_3 are calculated based on the X-ray density $\rho(x)$, table 1 [7]. The quantities $M_0(x)$ are calculated for the spin $s = 3/2$ by the formula (16).
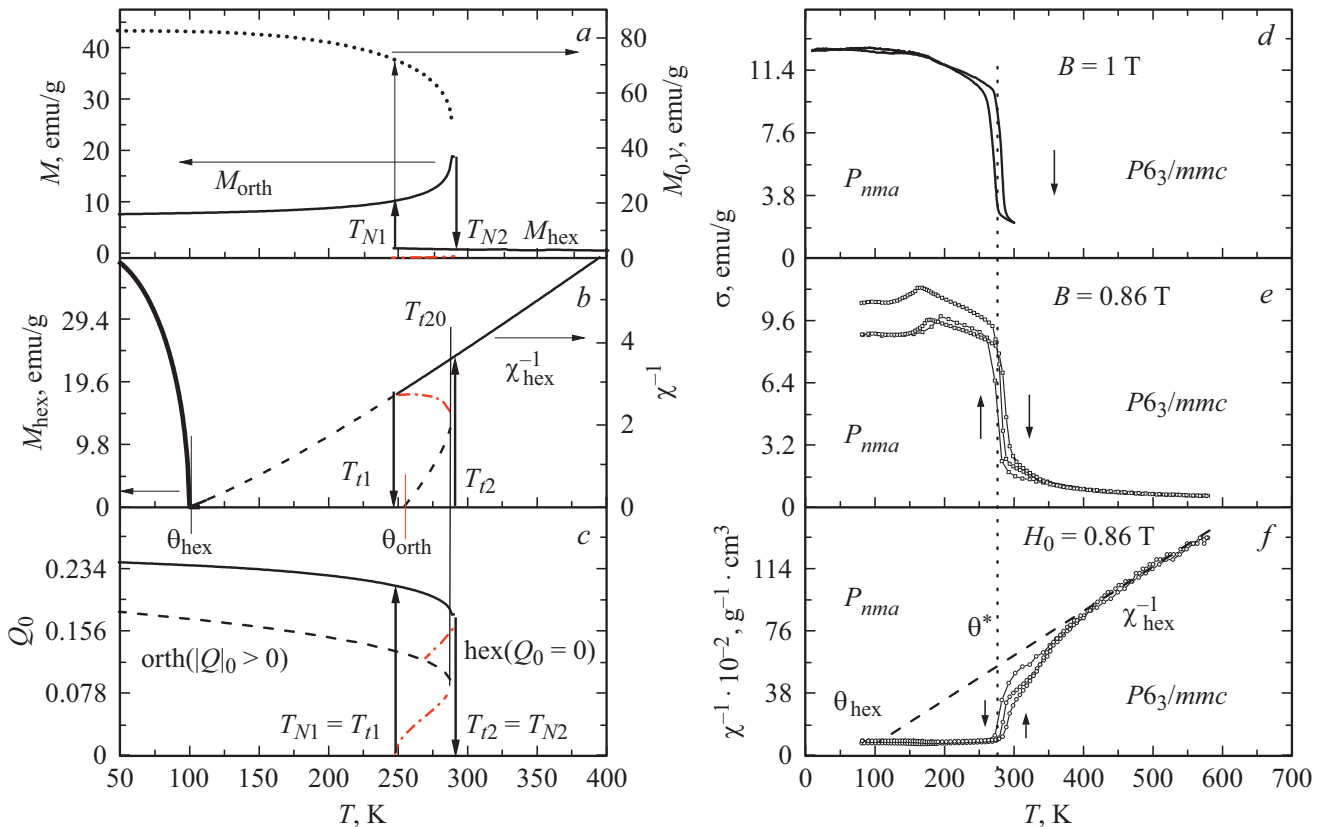

Figure 1. Theoretical (a, b, c) and experimental (d, e, f) temperature dependences of the magnetostructural characteristics in the $Mn_{0.95}Co_{0.05}NiGe$ solid solution in weak magnetic fields (up to 1 T).
Dash-dotted lines here (Figs 1, *b* and 1, *c*) and further correspond to the maximum TP; vertical arrows mark lability temperatures of rhombic T_{t2} (hexagonal T_{t1}) phase in a field with induction $B = 1$ T; the dashed lines in Fig. 1, *c* describe the solutions of equations (12) for $Q_0(T)$, at $y(T) \equiv 0$ with the corresponding lability temperatures of the rhombic T_{t20} and hexagonal $T_{t10} \approx T_{t1}$ phases; y — helimagnetic order parameter in fields with induction $B = 1$ T (a); M_{orth}, M_{hex} — specific magnetizations in rhombic, hexagonal phases in a field with induction $B = 1$ T.
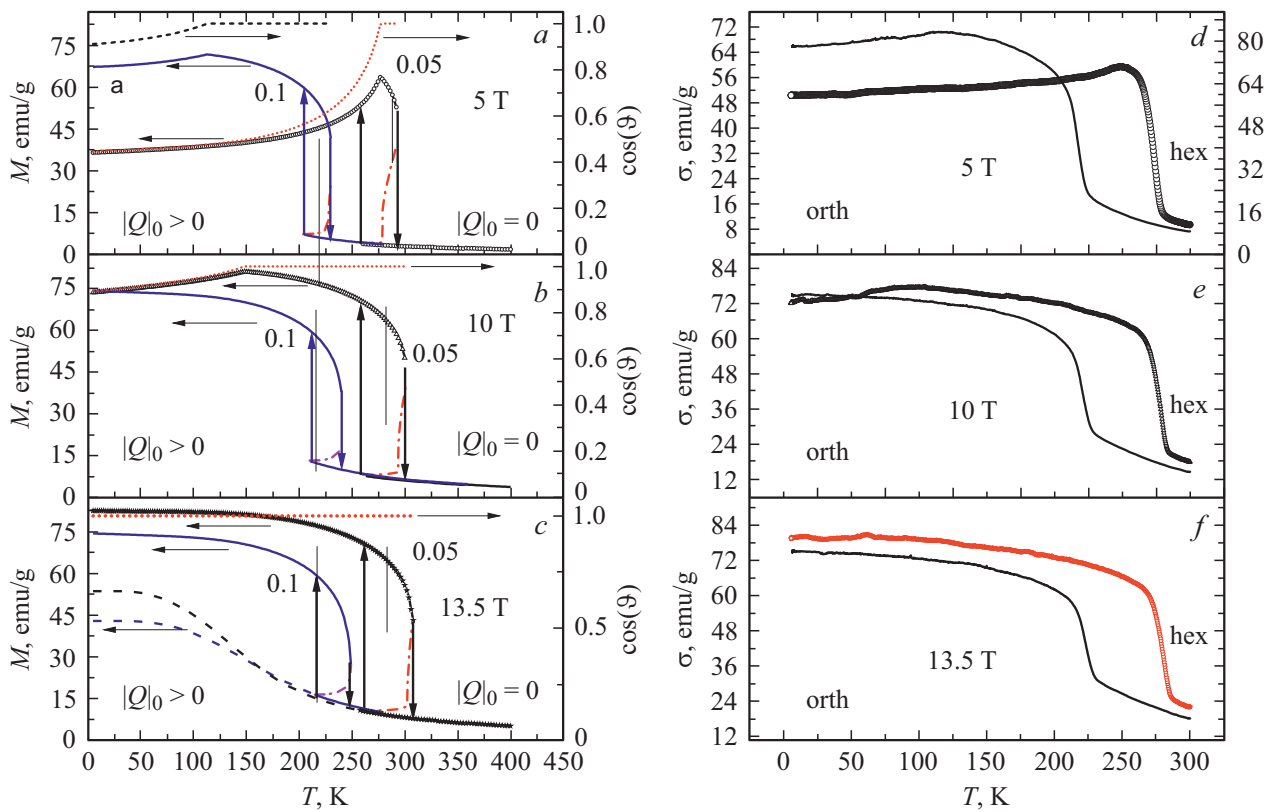
Figure 2. Temperature dependences of the magnetization of Mn$_{0.95}$Co$_{0.05}$NiGe (symbols) and Mn$_{0.9}$Co$_{0.1}$NiGe (lines) samples in strong magnetic fields. (*a, b, c*) — model; (*d, e, f*) — cooling experiment; vertical lines with arrows down (T_{t2}) and up (T_{t1}) determine the lability temperatures of the rhombic orth[$P_{nma}(Q_0 \neq 0)$] and hexagonal hex[$P6_3/mmc(Q_0 = 0)$] states during heating and cooling, respectively; thin vertical lines in the area of temperature hysteresis $\Delta T = T_{t2} - T_{t1}$ determine the temperatures T_m of the TP equality in the hexagonal and rhombic states in the corresponding fields; the dashed lines correspond to the continuation of the dependences of the magnetization in the hexagonal phase $M_{\text{hex}}(T) = M_0 y(T, Q_0 \equiv 0) \cos[\vartheta(T, Q_0 \equiv 0)]$ is below the lability temperature T_{t1} of the state with hexagonal configuration.

correlates with an increase in magnetization in Fig. 2, *a, b, c*. The theoretical results are in satisfactory agreement with the experimental ones shown in Fig. 2, *d, e, f*. It should be noted that the real temperature of magnetostructural ordering T_1 lies between the temperature of loss of stability of the hexagonal phase T_{t1} and the temperature of the TP equality in the rhombic and hexagonal states T_m. Depending on the physical and mechanical state of the crystal, the temperature T_1, apparently, can approach its limit value T_{t2} with increasing magnetic field induction.

The transition to a theoretical analysis of the properties of samples with $x \geq 0.15$ is carried out by changing the ratio between the coefficients responsible for the stabilization of the rhombic and hexagonal configurations in favor of the hexagonal one. In general, according to the table, this is due to a decrease in the value of $\nu_0(x)$ and an increase in the value of O(x). As an example, let us review the simulation of the temperature dependences of the magnetostructural characteristics of two samples with $x = 0.15$ and $x = 0.2$ in relatively weak magnetic fields ($B \leq 5$ T), Fig. 3 and in a strong field $B = 10$ T, Fig. 4.

The theoretical results shown in Fig. 3 correspond to the second scenario of the system behavior, in which the order-disorder transitions are isostructural transitions of the second order hex(FM) $\leftrightarrow$ hex(PM). Nevertheless, in this case, at temperatures below the magnetic ordering temperature ($T < \theta_{\text{hex}}$), the model admits the existence of a rhombic HM state, since the lability temperature of the rhombic state is $T_{t2} > 0$ (Fig. 3, *a, b*). The transition to the rhombic state is spontaneously difficult because, according to the calculations, the temperature of the appearance of this state is $T_{t1} < 0$. However, since the temperature $T_m(B)$ of the TP equality in the competing hexagonal ferromagnetic hex(FM) and rhombic helimagnetic orth(HM) states is positive ($0 < T_m < T_{t2}$), the transition to the rhombic phase in the ZFC mode is thermodynamically possible upon slow cooling to $T < T_m$. In this case, such a transition should be accompanied by volume deformations e_1 and a decrease in the magnetization Fig. 3, *b*.

This result gives an understanding of the low-temperature features of the temperature dependences of the magnetization in the ZFC-FC mode in increasing magnetic fields (Fig. 3, *c*). Indeed, on the one hand, the appearance of an
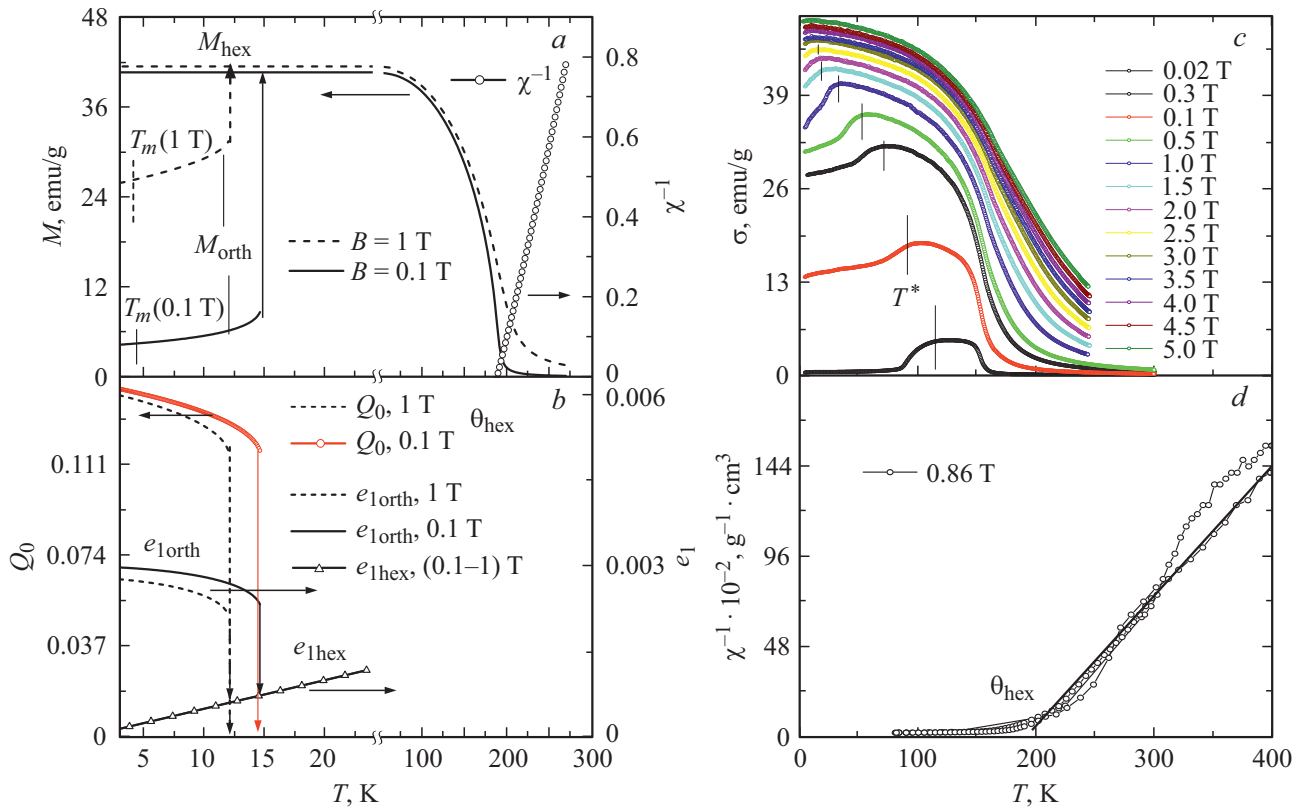
Figure 3. Temperature dependences of the magnetic and structural characteristics of the $Mn_{0.85}Co_{0.15}NiGe$ sample in magnetic fields up to 5 T. a, b — model; vertical arrows correspond to lability temperatures $T_{t2}(B)$ of the rhombic state; c, d — experiment, vertical lines $T^*(B)$ are put in correspondence with $T_{t2}(B)$; low-temperature magnetization in the ZFC mode corresponds to the magnetized AF phase in the rhombic state AF(orth) at $T < T_{t2}(B)$; $T_m(B)$ — is defined by $\Omega(|Q_0| > 0, y, B, T) = \Omega(0, y, B, T)$; and may correspond to the temperature of the transition to the rhombic state AF(orth).

orthorhombic phase is associated with the appearance of a helimagnetic state and an antiferromagnetic contribution to the magnetization. On the other hand, the appearance of bulk deformations e_1 of the crystal cell accompanying hex(FM) $\leftrightarrow$ orth(HM) transitions leads to additional obstacles for the formation of nuclei of new phases [8]. This can become a decisive factor for blocking reversible magnetostructural processes in a magnetic field at low temperatures and for maintaining the FM states induced by a magnetic field. Or in other words, to the opportunity of realizing low-temperature irreversible induced transitions described in Figs 5, a–5, f) and experimentally fixed in Fig. 6.

In more detail, the process of implementing irreversible field-induced transitions is as follows. When the sample temperature is lowered in the ZFC mode to $T < T_m$, the helimagnetic rhombic state HM(orth) is realized with a lower value of TP ($\Omega_{orth} < \Omega_{hex}$, Fig. 5, c, Fig. 5, f). The primary process of magnetization of the HM(orth) state is described by a thick line in Fig. 5, a, d. The break field of these lines B_1 corresponds to the complete suppression of the helimagnetic state and the appearance of the „weakly ferromagnetic" rhombic state FM(orth), which persists up to $B = B_2$. The field B_2 corresponds to the field lability

boundary of the „weakly" ferromagnetic rhombic state. The values of B_2 are compared with the experimental values of B_{k1} (Fig. 6) for real diffuse induced transitions. Thus, the induced transition at $B = B_{k1}$, according to our theory, is a magnetostructural transition of the 1st order FM(orth)−FM(hex) type, which is accompanied by abrupt changes in volumetric deformations e_1 and magnetic (y) and structural (Q_0) order parameters, Fig. 5, b, c, e, f. These transitions owe their existence to the difference in saturation magnetization values in the ferromagnetic rhombic $M_{orth} = M_0 y_{orth}$ and hexagonal $M_{hex} = M_0 y_{hex} > M_{orth}$ states. Note that for $O(x) = 0$, $M_{hex}(T = 0) = M_{orth}(T = 0)$ since for $T = 0$ according to (12b) $y_{orth} = y_{hex} = B_s(X) = 1$. The irreversibility of the field-induced hexagonal state, which is observed experimentally when the field is lowered and the sample is remagnetized (Fig. 6, a), can arise due to volume-structural blocking of the processes of nucleation of competing phases as a result of differences in specific volumes in rhombic and hexagonal states ($e_{1orth} > e_{1hex}$). Theoretically, this is realized due to the negative value of the lability temperature of the hexagonal ferromagnetic state ($T_{t1} < 0$) in the region of low values of the magnetic field induction ($B \ll B_2$). The differences between the model $M(B)$ and experimental $\sigma(B)$ dependences can be caused
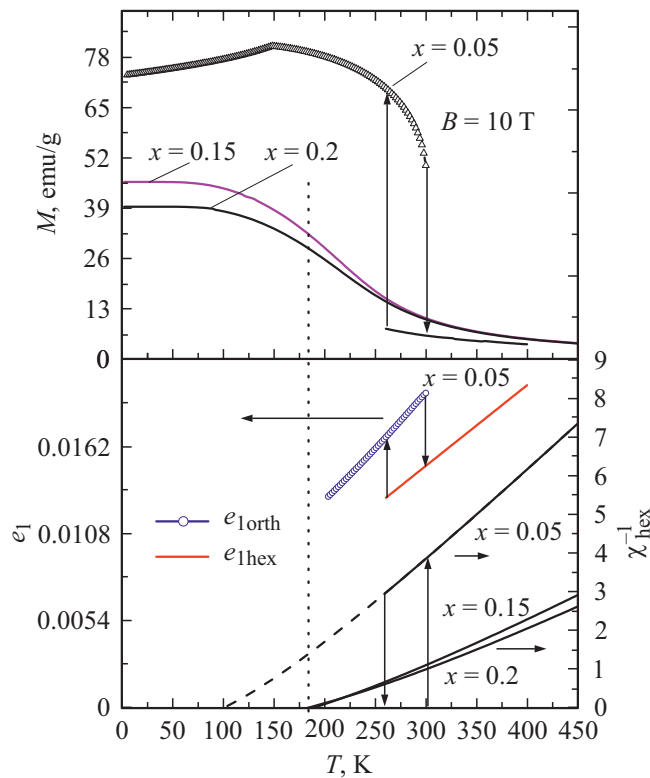
Figure 4. Theoretical dependences modeling the temperature peculiarities of the magnetization $M(T)$, inverse paramagnetic susceptibility $\chi^{-1}(T)$ and relative volume $e_1(T)$ of the corresponding alloys of the system under study in a strong magnetic field $B = 10$ T.

by the use of a single-domain description of magnetostructural phenomena and the geometry of the external field induction direction ($\mathbf{B}//\mathbf{q}$). In this case, the olicrystalline sample used is considered as a single-crystal single-domain, in which the processes of rotation of magnetocrystalline domains when approaching the saturation magnetization are not taken into account.

3. Magnetocaloric peculiarities

Expression for the system entropy

$$S(T, H_0) \equiv S[Q_0(T, H_0), y(T, H_0), T]$$

can be obtained from the definition of $S = -\partial\Omega/\partial T$ and reduced to the form

$$S[T, H_0] = N_0 k_B \ln\left\{z\left[X[Q_0(T, H_0), y(T, H_0), T]\right]\right\}$$

$$- N k_B B_s(X) X[Q_0(T, H_0), y(T, H_0), T] + \alpha k_0 e_1$$

$$\times [Q_0(T, H_0), y(T, H_0), T] + \frac{1}{2} N_0 k_B \ln[\sigma(Q_0(T, H), T)]. \quad (17)$$

In (17), the first two terms correspond to the entropy of a magnetically ordered system of spins in rhombic —

$Q_0 \neq 0$ (hexagonal $Q_0 = 0$) by crystal lattices for a given temperature: 3rd term — entropy of a volumetrically deformed magnetically ordered crystal in rhombic (hexagonal) states; the last term describes the decrease in the entropy of the crystal due to the appearance of a structural order parameter Q_0. The temperature dependences $[\Delta S(T)] = [S(B = \mu_0 H_0) - S(0)]$ are shown in Fig. 7 and correspond to heating (air magnetic permeability $\mu_0 = 1$).

Analysis of these dependencies calculated as part of the model used for the values of the orthogonal field: $sO/k_B = 282.5$ K, $sO/k_B = 382.5$ K, $sO/k_B = 467.5$ K for $x = 0.05$, $x = 0.1$ and $x = 0.15$ respectively, shows that for samples $x = 0.05$, $x = 0.1$ the maximum change in the isothermal entropy $\Delta S(T)$ corresponds to the direct MCE and the temperature region of magnetostructural 1st order transitions order-disorder orth(HM) $\leftrightarrow$ hex(PM), which in strong fields in full accordance with the experimental data are transformed into orth(FM) $\leftrightarrow$ hex(PM) transitions (Fig. 2, e, f). The discrepancy between the theoretical and experimental dependences is due to two factors. First of all, these are the diffuse nature of magnetostructural phase transitions, which is not taken into account in the present theoretical description, the use of the isotropic form of magnetoelastic energy [8] and approximate values of a number of elastic constants, for example, compressibility ($\kappa(x) = 1/k_0 = 2 \cdot 10^{-3}$ kbar^{-1}) and volume expansion coefficient ($\alpha(x) = 2 \cdot 10^{-5}$ [$^\circ$K]$^{-1}$).

For a sample with $x = 0.15$, the maximum values of the isothermal entropy $\Delta S(T)$ (Fig. 7, f) as a reaction to the inclusion of a magnetic field when the sample is heated correspond to the lability temperatures of the rhombic state $T_{t2}(0)$, $T_{t2}(B)$ under transitions orth(HM) $\leftrightarrow$ hex(FM) in Fig. 2, Fig. 7, e. The temperature value T_{t2} correlates with the temperature value T^* in Fig. 3, c. The qualitative behavior of the quantities T^* and T_{t2} with an increase in the induction intensity agrees with — their values decrease with an increase in the magnetic field. However, the value $T^* > T_{t2}(0)$ shall be brought as to fully correspond to the values of these quantities and the quantities B_2 (Fig. 5) and B_1 (Fig. 6) into full correspondence. The value $\Delta S(T) > 0$ in the temperature range $T < T_{t2}(0)$ determines the inverse magnetocaloric effect (IMCE). It can be observed only in fields $B < B_2$ ($B < B_{k1}$), since in high fields the sample is already in a stable hexagonal ferromagnetic state hex(FM) and subsequent temperature changes in the field or field at a constant temperature will not lead to a sharp increase in magnetization and, accordingly, ΔS in the area of helium temperatures. However, the direct magnetocaloric effect (DMCE) can be observed at high temperatures. DMCE in samples with $x \geq 0.15$ should be observed in the area of isostructural magnetic disorder and reach a maximum at the Curie temperature. In the model description in Fig. 7 this is $T = \theta_{hex}$. A more realistic process of the appearance of IMCE for samples with $x \geq 0.15$ can be tracked by considering not temperature, but field dependences of the jump in entropy $\Delta S(B)$ at a fixed temperature. Figure 8 shows
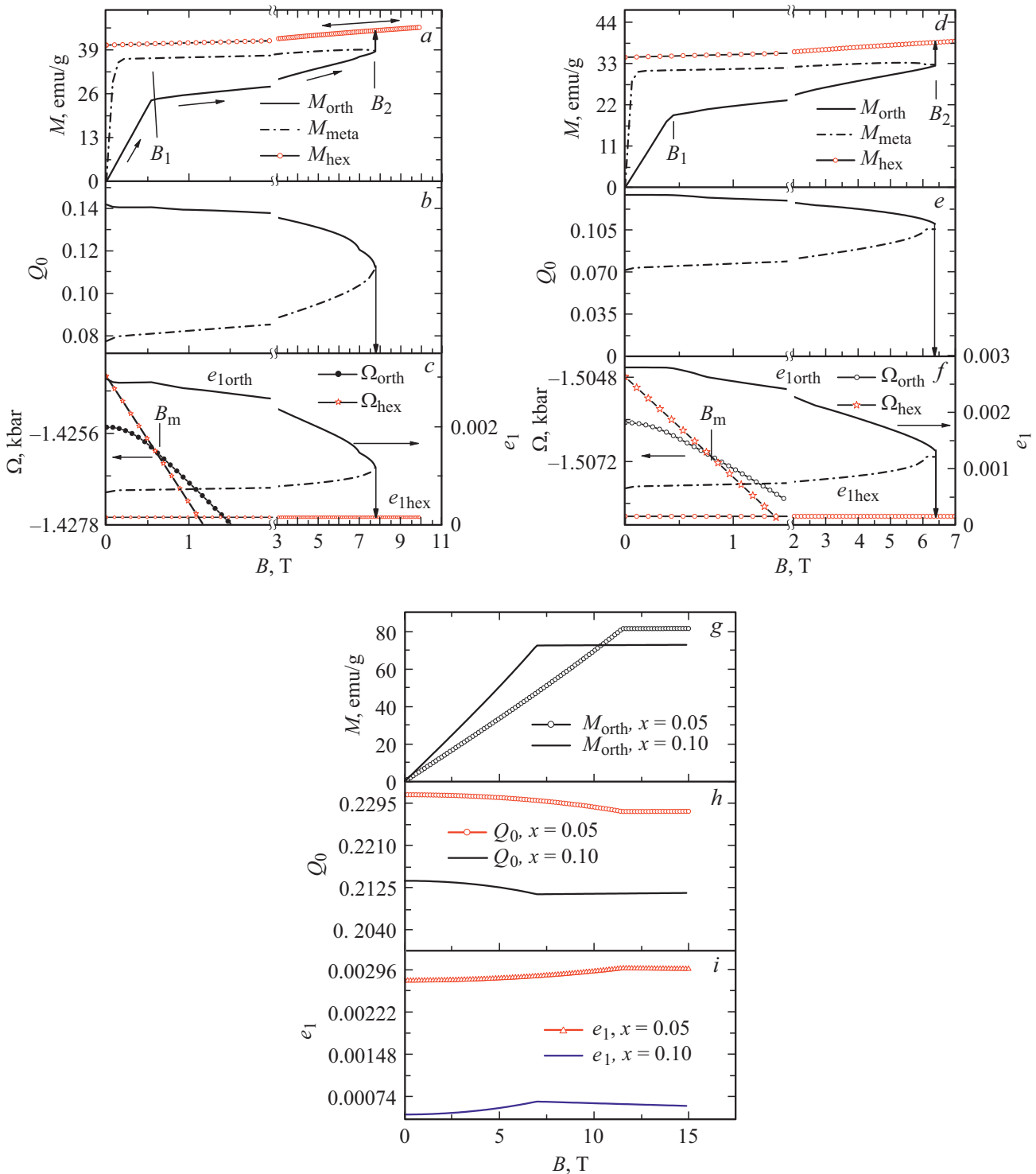
Figure 5. Model field dependences of magnetization — M, structural order parameter — Q_0, volumetric strains — e_1, explaining the mechanism of irreversible $a-f$ and reversible $g-i$ field-induced transitions. Kinks $M(B)$ correspond to the suppression of the helimagnetic state and the appearance of a ferromagnetic state in the rhombic lattice; vertical arrows mark the field boundaries of the lability of the rhombic state — FM(orth) at irreversible transitions FM (orth)−FM (hex).
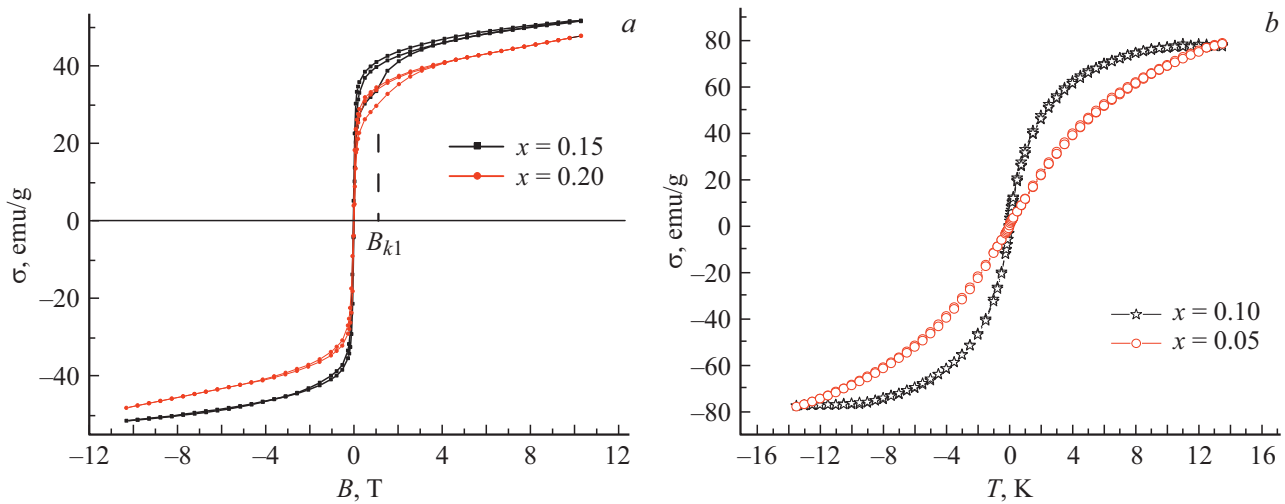
Figure 6. Experimental field dependences of the magnetization of a number of samples of the system under study at $T = 5$ K. Dependences $\sigma(B)$ for $x = 0.15$ and $x = 0.2$ can be interpreted as irreversible magnetostructural transitions induced by a magnetic field from a weakly ferromagnetic rhombic to a ferromagnetic hexagonal state; the dependences $\sigma(B)$ for $x = 0.05$ and $x = 0.1$ are typical for a smooth isostructural increase in magnetization that accompanies the suppression of a helimagnetic rhombic structure by a magnetic field.

the model field dependences of the isothermal entropies $S(B)$ for the rhombic $S_{orth}(B)$ and hexagonal $S_{hex}(B)$ phases and change in the jump in isothermal entropy $\Delta S(B) = S(B) - S(0)$, combined with $M(B)$ dependences for a sample with $x = 0.15$ at a temperature 3 K. In the field $B < B_2$ $\Delta S(B) = S_{orth}(B) - S_{orth}(0) \leq 3.2$ J/K · kg describes the inverse MCE, which corresponds to the isostructural stabilization of the ferromagnetic state as the magnetization increases from its value in the helimagnetic state HM(orth) $(B \leq B_1)$ to its maximum value in rhombic state FM(orth) $(B \leq B_2)$. Irreversible jump $\Delta S(B) = S_{hex}(B) - S_{orth}(0) = 7.5$ J/K · kg at $B = B_2$ corresponds to the irreversible magnetostructural transition FM(orth) $\leftrightarrow$ FM(hex), Fig. 8, *a*. Here, irreversibility means that in order to repeat the process of primary magnetization, it is required to heat the sample aver the temperature of $T_{t2}(0)$ and then cool it in the ZFC mode.

Large-scale changes in the $\Delta S(T)$ values during magnetostructural transitions are related to the fact that the decrease in the symmetry of the system due to the appearance of magnetic order correlates with the decrease in the symmetry of the crystal lattice from more symmetric hexagonal to less symmetric rhombic. This leads to the fact that changes in the purely magnetic contribution from the first two terms in (17) are supplemented by changes in the structural contribution from the last term in (17).

Meanwhile, an increase in volumetric strains in the rhombic state, on the contrary, weakens the first two contributions. Therefore, to enhance the magnitude of the magnetocaloric effect (MCE), it is advantageous to achieve compensation for volumetric strains. Because the contributions to $\Delta S(T)$ from the change in volume and from the change in the crystal structure have different signs. This can be achieved by selecting the appropriate doping with an increase in the number of components of the basic composition. Such doping should lead to the maximum compensation of volumetric strains while maintaining the jumps in lattice parameter strains, which provide magnetostrictive contributions to the jump-like implementation of magnetic ordering. A more detailed analysis of the relationship between volumetric strains and spontaneous magnetostriction in layered structures can be found in [9].

4. Conclusion

The work shows that taking into account changes in the effective exchange integrals and the internal orthogonal field with a change in the structural configuration of atomic centers and the concentration of Co underlies the formation of the mechanism of magnetostructural coupling between the spin and lattice subsystems of solid solutions Mn$_{1-x}$Co$_x$NiGe. As part of this approach, using the mean field approximation for the spin subsystem and the shifted harmonic oscillator approximation for the structural subsystem, there is an interpretation of two scenarios for the implementation of magnetic disordering and features of a jump change in the saturation magnetization at helium temperatures. A qualitative agreement is obtained between the behavior of the experimental and theoretical magnetic and magnetocaloric characteristics in the area of room temperatures. The existence of an inverse magnetocaloric effect, enhanced by a magnetostructural transition, is predicted at helium temperatures.
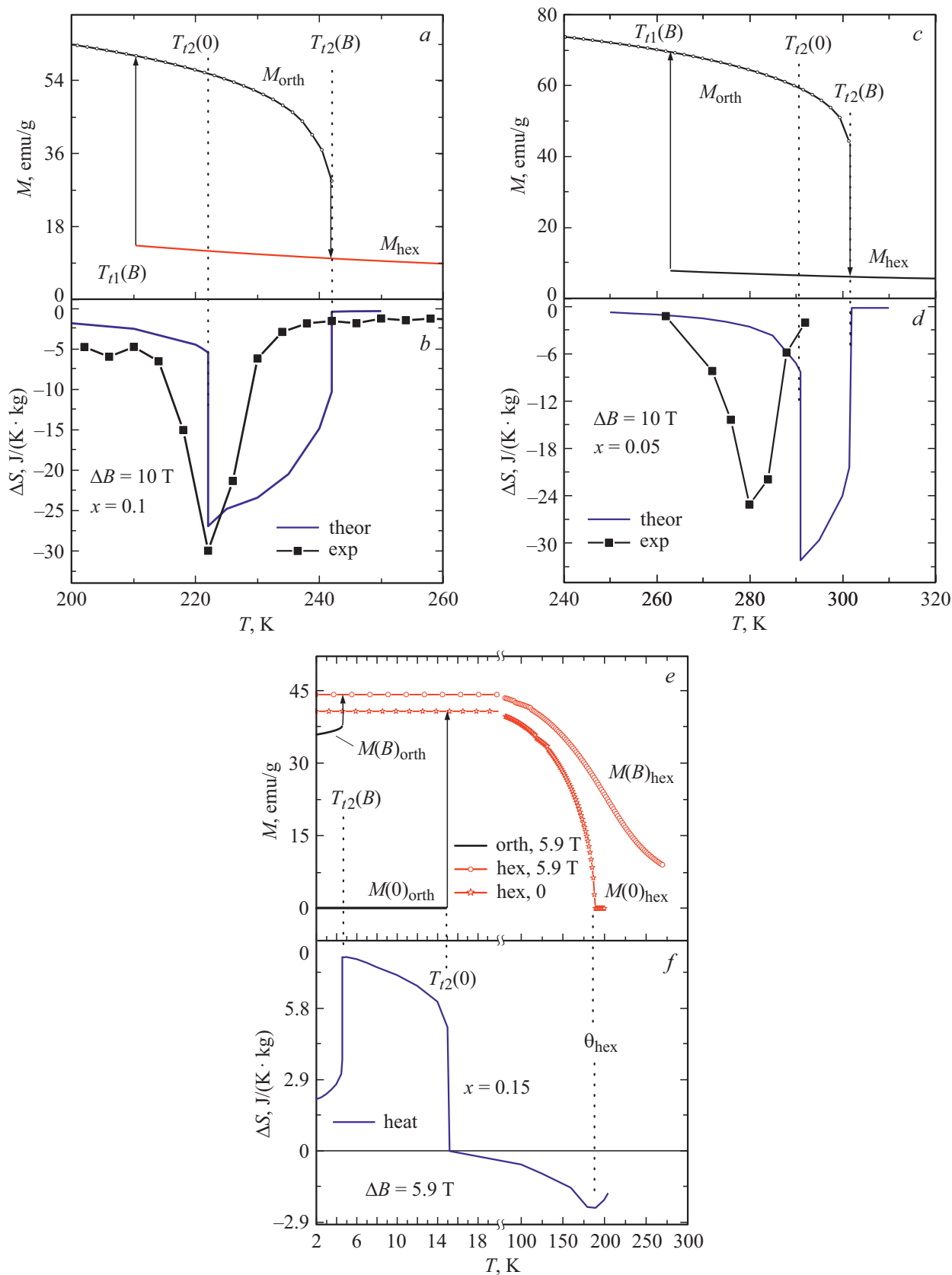
Figure 7. Combined experimental and theoretical temperature dependences of the change in magnetic entropy and magnetization $M(T)$ with an isothermal change in the magnetic field. Demonstrate high-temperature direct MCE (b, d, f), and low-temperature reverse MCE (f); $T_{t2}(0)$ and $T_{t2}(B)$ correspond to the lability temperatures of the rhombic state in a field with induction $B = 0$ and $= 10$ T ($a-c$), $B = 5.9$ T (e, f, theory) in FM(orth)−FM(hex) transitions.
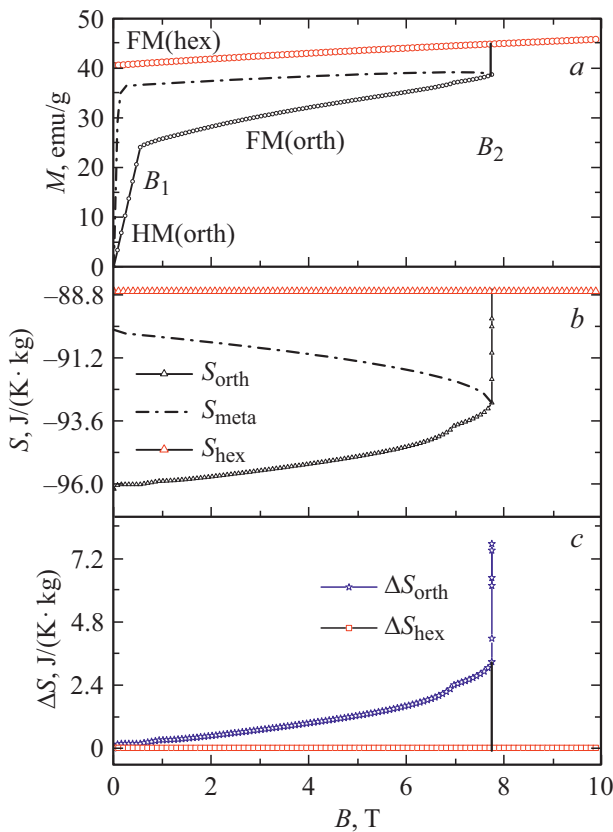
Figure 8. Theoretical field dependences of magnetization $M(B)$, magnetic entropy $S(B)$ and $\Delta S(B)$ in the area of reversible HM(orth)−FM(orth) and irreversible FM(orth)−FM(hex) transitions. They demonstrate the peculiarities of the implementation of the inverse low-temperature MCE $\Delta S \equiv \Delta S(B) = S(B, T) - S(0, T)$ at $T = 3\,\mathrm{K}$ in a sample with $x = 0.15$.

Appendix

In the mean field approximation (MFA) (3) can be represented in the form

$$\hat{H}_{\mathbf{h}}(s) = -\sum_{nk} \Delta_n^k \hat{s}_n^k, \qquad (A1)$$

where $\Delta_n^k = \mathbf{h}_n^k + \mathbf{O}_n^k$.

In (A1), like MFA, operators $\sum_{nk,n'k'} J_{nn'}^{kk'} \hat{s}_n^k \hat{s}_{n'}^{k'} + 2\mu_B \mathbf{H}_0 \sum_{ni} \hat{s}_n^k$ from (3), including multiparticle interactions $\sum_{nk,n'k'} J_{nn'}^{kk'} \hat{s}_n^k \hat{s}_{n'}^{k'}$, are replaced by the operators of $\left(\sum_{n,k} \mathbf{h}_n^k \hat{s}_n^k\right)$ single-particle interaction. Meanwhile, the orthogonality condition is introduced for the exchange $\mathbf{h}_n^k = h\mathbf{u}_n^k$ and the internal space-periodic $\mathbf{O}_n^k = O\mathbf{w}_n^k$ fields

$$\mathbf{O}_n^k \mathbf{h}_n^k = (\mathbf{w}_n^k \mathbf{u}_n^k) O h = 0. \qquad (A3)$$

In (3) there are O, h-modules of internal space-periodic and exchange fields.

For a simple space-periodic helimagnetic spin structure with the structure wave vector $\mathbf{q} = [0, 0, q_a]$, the unit vectors $\mathbf{w}_n^k \mathbf{u}_n^k$ satisfying the orthogonality condition (A3) can be represented in the form

$$\mathbf{u}_n^k = \left[\cos(\mathbf{q}\mathbf{R}_n^k)\sin(\vartheta), \sin(\mathbf{q}\mathbf{R}_n^k)\sin(\vartheta), \cos(\vartheta)\right], \quad (A4a)$$

$$\mathbf{w}_n^k = \left[\sin(\mathbf{q}\mathbf{R}_n^k), -\cos(\mathbf{q}\mathbf{R}_n^k), 0\right], \qquad (A4b)$$

$\mathbf{u}_n^k$ coincides with the direction of the local quantization axis, which at $H_0 = 0$ is in the plane perpendicular to the wave vector $\mathbf{q}$ ($\vartheta = \pi/2$). Distribution function

$$\rho(\hat{H}_h) = \prod_{n,k} \rho_n^k(\hat{H}_h) \equiv \prod_{n,k} \rho_n^k(\hat{M}_n^k)$$

as part of the MFA with Hamiltonian (A1) is the product of single-particle distribution functions $\rho_n^k(\hat{H}_h) \equiv \rho_n^k$

$$\rho_n^k(\hat{M}_n^k) \equiv \rho_n^k = \frac{e^{\beta|\mathbf{h}_n^k + \mathbf{O}_n^k|\mathbf{V}_n^k \hat{s}_n^k}}{z(X)} \equiv \frac{e^{\beta\sqrt{h^2 + O^2}\hat{M}_n^k}}{z(X)}, \qquad (A5)$$

$$z(X) = Sp\, e^{\beta(\sqrt{h^2 + O^2})\hat{M}_n^k} \equiv \sum_{M_n^k = -s}^{s} e^{\beta(\sqrt{h^2 + O^2})M_n^k}$$

$$= \mathrm{sh}[(1 + (2s)^{-1})X] / \mathrm{sh}[(2s)^{-1}X], \qquad (A6)$$

$$X = \beta s\sqrt{h^2 + O^2}, \quad \beta = 1/k_B T, \quad M_n^k \in -s, s+1, \ldots, s,$$

where $\hat{M}_n^k$ is the spin projection operator on the direction $\mathbf{V}_n^k$ of the molecular field Δ_n^k

$$\Delta_n^k = \mathbf{h}_n^k + \mathbf{O}_n^k = \Delta\mathbf{V}_n^k \equiv |(\mathbf{h}_n^k + \mathbf{O}_n^k)|\mathbf{V}_n^k \equiv \left(\sqrt{h^2 + O^2}\right)\mathbf{V}_n^k,$$

which is determined by the unit vector $\mathbf{V}_n^k$, M_n^k by the operator eigenvalue of $\hat{M}_n^k$.

The quantity $h \equiv h(\mathbf{q})$ is a variational parameter, which is determined using the variational principle of statistical mechanics: the optimal value of the quantity h should satisfy the extreme value of the model free energy Ω_M.

Model free energy

$$\Omega_M \equiv Q_M(H(s))$$

as the upper limit of the genuine free energy $\Omega(\hat{H}(s)) \equiv \Omega$ of the spin system is given by the expression [1,2,10]

$$\Omega_M = \langle \hat{H}(s) - \hat{H}_{\mathbf{h}}(s) \rangle_{\hat{H}_h} - N k_B T \ln z(X). \qquad (A7)$$

The average

$$\langle \hat{H}(s) - \hat{H}_{\mathbf{h}}(s) \rangle_{\hat{H}_h} \equiv \langle \hat{H}(s) - \hat{H}_{\mathbf{h}}(s) \rangle$$

is determined according to the following diagram

$$\left\langle -\sum_{nk,n'k'} J_{nn'}^{kk'} \hat{s}_n^k \hat{s}_{n'}^{k'} - 2\mu_B \mathbf{H}_0 \sum_{ni} \hat{s}_n^k + \sum_{ni} \hat{s}_n^k \mathbf{h}_n^k \right\rangle$$

$$\equiv -\sum_{nk,n'k'} J_{nn'}^{kk'} \langle \hat{s}_n^k \rangle \langle \hat{s}_{n'}^{k'} \rangle - 2\mu_B \mathbf{H}_0 \sum_{ni} \langle \hat{s}_n^k \rangle + \sum_{ni} \langle \hat{s}_n^k \rangle \mathbf{h}_n^k.$$

$$(A8)$$

In the spin subsystem under consideration, three types of averages can be distinguished

$$\langle \hat{s}_n^k \rangle_W = \mathbf{w}_n^k \langle \mathbf{w}_n^k \hat{s}_n^k \rangle = \mathbf{w}_n^k \langle \hat{\mathbf{l}}_n^k \rangle = \mathbf{w}_n^k l, \qquad (A9a)$$

$$\langle \hat{s}_n^k \rangle_V = \mathbf{V}_n^k \langle \mathbf{V}_n^k \hat{s}_n^k \rangle = \mathbf{V}_n^k \langle \hat{\mathbf{M}}_n^k \rangle = \mathbf{V}_n^k M, \qquad (A9b)$$

$$\langle \hat{s}_n^k \rangle_u = \mathbf{u}_n^k \langle \mathbf{u}_n^k \hat{s}_n^k \rangle = \mathbf{u}_n^k \langle \hat{\mathbf{m}}_n^k \rangle = \mathbf{u}_n^k m, \qquad (A9c)$$

where $l \equiv \langle \hat{\mathbf{l}}_n^k \rangle = \langle \mathbf{w}_n^k \hat{s}_n^k \rangle$, $M = \langle \hat{\mathbf{M}}_n^k \rangle = \langle \mathbf{V}_n^k \hat{s}_n^k \rangle$, $m = \langle \hat{\mathbf{m}}_n^k \rangle = \langle \mathbf{u}_n^k \hat{s}_n^k \rangle$ — average values of projection operators of the spin operator $\hat{s}_n^k$ onto the directions of the corresponding fields.

Thus, (A9a)−(A9c) correspond to the mean values of the components of the spin operator along the internal periodic field (A9a), along the mean field (A9b), and along the exchange field (A9c), which forms the local quantization axis. From this set, using the distribution function $\rho_n^k(\hat{\mathbf{M}}_n^k)$ (A5), only $\langle \hat{s}_n^k \rangle_V = \mathbf{V}_n^k \langle \hat{\mathbf{M}}_n^k \rangle$ can be calculated directly.

$$\langle \hat{s}_n^k \rangle_V = \mathbf{V}_n^k \langle \hat{\mathbf{M}}_n^k \rangle = \mathbf{V}_n^k Sp \frac{\hat{\mathbf{M}}_n^k e^{\beta(\sqrt{h^2+O^2})\hat{\mathbf{M}}_n^k}}{z(X)}$$

$$= \mathbf{V}_n^k \sum_{M_n^k=-s}^{s} \frac{M_n^k e^{\beta(\sqrt{h^2+O^2})M_n^k}}{z(X)} = \mathbf{V}_n^k s B_s(X) \equiv \mathbf{V}_n^k M,$$
$$(A10)$$

where the Brillouin function $B_s(X)$ is defined by the expression

$$B_s(X) = \left(\frac{1}{2s+1}\right) \coth \frac{1}{2s+1} X - \left(\frac{1}{2s}\right) \coth \frac{1}{2s} X.$$
$$(A11)$$

It can be shown that the remaining mean values of $\langle \hat{\mathbf{l}}_n^k \rangle$, $\langle \hat{\mathbf{m}}_n^k \rangle$ are not independent and are expressed in terms of the component M. To do this, we reduce the equality

$$\left\langle (\mathbf{h}_n^k + \mathbf{O}_n^k)\hat{s}_n^k \right\rangle = \left\langle \mathbf{V}_n^k \hat{s}_n^k \sqrt{h^2+O^2} \right\rangle$$

to the form

$$h \langle \hat{\mathbf{m}}_n^k \rangle + \mathbf{O} \langle \hat{\mathbf{l}}_n^k \rangle = M \sqrt{h^2+O^2}. \qquad (A12)$$

Taking in turn the partial derivatives $\partial/\partial O$ and $\partial/\partial h$ of both parts (A12) we get

$$\langle \hat{\mathbf{l}}_n^k \rangle = \frac{O}{\sqrt{h^2+O^2}} M \equiv l,$$

$$\langle \hat{\mathbf{m}}_n^k \rangle = \frac{h}{\sqrt{h^2+O^2}} M \equiv m \equiv ys. \qquad (A13)$$

It should be noted that for $O \neq 0$ only $\langle \hat{s}_n^k \rangle_u$ are measured quantities, so as average (A8) $\langle \hat{s}_n^k \rangle$ we use the measured quantities $\langle \hat{s}_n^k \rangle_u$. Taking into account, according to (A13), the computability m and the representation of the measured

quantity $\langle \hat{s}_n^k \rangle_u$ in the form $\langle \hat{s}_n^k \rangle_u = \mathbf{u}_n^k m$ the expression Ω_M can be reduced to the form

$$\Omega_M = -\sum_{n,k} \left[\left[m^2 \sum_{n',k'} J(|\Delta\mathbf{R}_{nn'}^{kk'}|) \mathbf{u}_n^k \mathbf{u}_{n'}^{k'} \right] + 2\mu_B \mathbf{H}_0 \mathbf{u}_n^k m - mh \right]$$

$$- Nk_BT \ln[z(X)] = -Nm^2 \left[J(q_0) \sin^2(\vartheta) + J(0) \cos^2(\vartheta) \right]$$

$$- N2\mu_B H_0 \cos(\vartheta) m + Nmh - Nk_BT \ln[z(X)],$$
$$(A14a)$$

$$J(q_a) = \sum_{\Delta\mathbf{R}} J(|\Delta\mathbf{R}|) \cos(\mathbf{q}\Delta\mathbf{R})$$

$$\approx J_0 + J_1 \cos(\Psi) + J_2 \cos(2\Psi), \qquad (A14b)$$

$$J(0) \equiv J(q_a = 0) \equiv J(\Psi = 0) = J_0 + J_1 + J_2. \quad (A14c)$$

The expression for the modulus of the exchange field is determined from the condition

$$d\Omega_M/dh = \partial\Omega_M/\partial h + (\partial\Omega_M/\partial m)dm/dh = 0. \quad (A15)$$

Meanwhile, since

$$\partial\Omega_M/\partial h = Nm - N\partial k_BT \ln z(X)/\partial h$$

$$= Nm - \frac{hN}{\sqrt{h^2+O^2}} M = 0$$

(see A13), then (A15) is reduced to the form

$$(dm/dh)\Big\{ -2m[J(q_a) \sin^2(\vartheta) + J(0) \cos^2(\vartheta)]$$

$$- 2\mu_B H_0 \cos(\vartheta) + h \Big\} = 0. \qquad (A16)$$

Where

$$h = \Big\{ 2[J(q_a)(\sin(\vartheta)^2) + J(0)(\cos(\vartheta)^2)]m + 2\mu_B H_0 \cos(\vartheta) \Big\}.$$
$$(A17)$$

After substituting (A17) into (A14a), the expression Ω_M in the form (5a) is obtained.

Funding

Conflict of interest

The authors declare that they have no conflict of interest.

References

[1] V.I. Val'kov, A.V. Golovchan, V.V. Koledov, V.I. Mityuk, I.F. Gribanov, V.D. Zaporozhets, B.M. Todris, T.S. Sivachenko. FTVD **29**, 5 (2019) (in Russian).

[2] V.I. Val'kov, A.V. Golovchan, V.V. Koledov, B.M. Todris, V.I. Mityuk. FTT **62**, *5*, 710 (2020) (in Russian).

[3] R. Blints, B. Zheksh. Ferroelectrics and antiferroelectrics. Lattice dynamics, Mir, M. (1975). 398 p.

[4] J.-T. Wang, D.-S. Wang, C. Chen, O. Nashima, T. Kanomata, H. Mizuseki, Y. Kawazoe. Appl. Phys. Lett. **89**, 262504 (2006).

[5] B. Penc, A. Hoser, S. Baran, A. Szytuła. Phase Transit. **91**, 118 (2018).

[6] E.K. Liu, H.G. Zhang, G.Z. Xu, X.M. Zhang, R.S. Ma. Appl. Phys. Lett. **102**, 122405 (2013).

[7] V.I. Mityuk, G.S. Rimskiy, V.V. Koledov, A.V. Mashirov, V.I. Val'kov, A.V. Golovchan, O.E. Kovalev. FTT **63**, *12*, 2021 (in Russian).

[8] S.K. Asadov, E.A. Zavadsky, V.I. Kamenev, E.P. Stefanovsky, A.L. Sukstansky, B.M. Todris. FTT **42**, *9*, 1649 (2000) (in Russian).

[9] V.I. Val'kov, A.V. Golovchan. FNT **39**, 904 (2013) (in Russian).

[10] S.V. Tyablikov. Metody kvantovoi teorii magnetizma, Nauka, M. (1975). 528 p. (in Russian).